Simulation Modelling Practice and Theory 16 (2008) 933–944

Contents lists available at ScienceDirect

Simulation Modelling Practice and Theory

journal homepage: www.elsevier.com/locate/simpat

Model based inertial sensing of human body motion kinematics in sit-to-stand movement

Josip Musić [a,*], Roman Kamnik [b], Marko Munih [b]

[a] University of Split, Faculty of Electrical Engineering, Mechanical Engineering and Naval Architecture, R. Boškovića bb, 21000 Split, Croatia
[b] University of Ljubljana, Faculty of Electrical Engineering, Tržaška 25, 1001 Ljubljana, Slovenia

ARTICLE INFO

Article history:
Received 4 January 2008
Received in revised form 14 March 2008
Accepted 9 May 2008
Available online 21 May 2008

Keywords:
Human body model
Inertial sensors
Standing-up

ABSTRACT

The paper presents the design and validation of a three-segment human body model. The model is aimed at the reconstruction of motion trajectories of the shank, thigh and HAT (Head-Arms-Trunk) segments in sit-to-stand-motion using low cost inertial sensors. For this purpose the Extended Kalman filter is applied for fusion of model data and data acquired through measurements. The simplifications, like motion constraint to sagittal plane, symmetry of movement and assumption of ideal joints are introduced in the model. Model validation was performed on simulated data and on measurements data acquired with the Optotrak optical motion analysis system. Obtained results are presented and discussed.

1. Introduction

Sit-to-stand movement is a common but demanding activity of daily living which is on average performed four times in an hour [4]. A standing-up maneuver requires coordination of several muscle groups with special requirements on balance [13]. This makes standing-up (and sitting down) difficult and challenging for persons who have lost part of lower limb functionality. A number of aiding systems have been developed for the purpose of standing-up support. Recently, robot assistive devices have been introduced and their benefits demonstrated [12]. In acquisition systems, the kinetic and kinematic parameters of the subject are required for operation of the robot control algorithm. Kinematic measurements are usually performed with optical motion analysis systems that are unsuitable for clinical applications. Optical motion analysis systems, although very accurate, have some drawbacks such as high cost, markers are easily obscured, low portability due to weight, need for an AC power supply and markers require time-consuming setting up procedure. Therefore, introduction of miniature, low cost inertial sensors (accelerometers and gyroscopes) as a body mounted sensors, has shown to be promising [3,11,15,21,23]. Because of their low cost and miniature size they are practical for a wide range of applications such as biomechanical analysis of human motion [3,7,11,15,23], virtual reality [21], ergonomics, navigation [10], etc. Inertial sensors are not without errors [3,7,15]: two accelerometer signal components, the dynamic and gravitational, cannot easily be distinguished during faster movements while drift of the gyroscope output results in large integration errors. The accuracy of inertial sensors can be improved by incorporation of additional measurement devices and by application of appropriate data fusion algorithms.

* Corresponding author. Tel.: +385 21 305 647; fax: +385 21 463 877.
E-mail addresses: jmusic@fesb.hr (J. Musić), roman.kamnik@robo.fe.uni-lj.si (R. Kamnik), marko.munih@robo.fe.uni-lj.si (M. Munih).

1569-190X/$ - see front matter © 2008 Elsevier B.V. All rights reserved.
doi:10.1016/j.simpat.2008.05.005

Three different approaches to human motion analysis using inertial sensors can be found in the literature:

(1) systems that use a single type of inertial sensors (either accelerometer or gyroscope) and are used in dedicated applications often providing more qualitative than quantitative information about human motion,
(2) systems that operate on the basis of a combination of accelerometers and gyroscopes with additional signal processing algorithms,
(3) systems that operate on a basis of both inertial sensor types in combination with additional sensors (usually magnetometers) and data fusion algorithms.

The most accurate measurements in human motion analysis are achieved by the third approach in which inertial sensors are used in conjunction with magnetometers and Kalman filtering techniques [18,21,23]. However, good measurement results are obtained under certain restrictions due to magnetometer high sensitivity to magnetic disturbances in Earth's local magnetic field [2,18]. The sources of Earth's local magnetic field disturbances can be ferrous materials (e.g. iron, nickel, steel, cobalt) in the vicinity of the sensor. In his research, Bachmann concluded that potential sources of magnetic disturbances should be at least 60 cm away from the magnetometers [2]. Since the intended application incorporates a robot assistive device for standing-up support it is reasonable to expect inertial sensor measurement errors due to corrupted magnetometer readings.

In the paper we assume that magnetometers can (in certain applications) be substituted by the incorporation of dynamic human body model. In the proposed approach the Extended Kalman filtering (EKF) technique is used to fuse data acquired from inertial sensor measurements with data from the dynamic human body model. In this way we believe that better kinematic measurements in ambulatory settings, where a number of ferrous material based objects and instruments (with their electromagnetic fields) exist, are possible. We named the approach Model Based Inertial Sensing – MoBIS.

The paper is organized as follows. In the second section, a three-segment dynamic human body model is constructed and described. The third section presents the design of the EKF which incorporates all necessary measurement data and data from the dynamic human body model with emphasis on accelerometer signal decomposition. In the fourth section the validation of constructed dynamic human body model and the proposed EKF structure is presented followed by the application of the proposed method on actual measurements of sit-to-stand movement. In section five, the discussion of obtained results is presented, while in the final section some conclusions are drawn based on observed method and model performance.

2. Dynamic human body motion model

The human body motion in sit-to-stand transfer can be approximated by motion of a three segment human body model in sagittal plane with three degrees of freedom of motion [9,12]. The kinematic variables of segments (angular positions $\dot{\Theta}_1$, $\dot{\Theta}_2$ and $\dot{\Theta}_3$, velocities $\dot{\Theta}_1$, $\dot{\Theta}_2$ and $\dot{\Theta}_3$, and accelerations $\ddot{\Theta}_1$, $\ddot{\Theta}_2$ and $\ddot{\Theta}_3$) uniquely define the sit-to-stand motion. In dynamic analysis of rigid body motion, the knowledge of translational and angular velocities and accelerations of body center of mass is crucial [19,20].

The proposed human body model consists of shank, thigh and HAT (Head-Arms-Trunk) segments as presented in Fig. 1. The segments are assumed to be rigid bodies with their masses contained at center of mass (CoM). Segment masses, lengths, moments of inertia and CoM positions are defined using anthropometric data [5]. Three joints (ankle, knee and hip) are as-

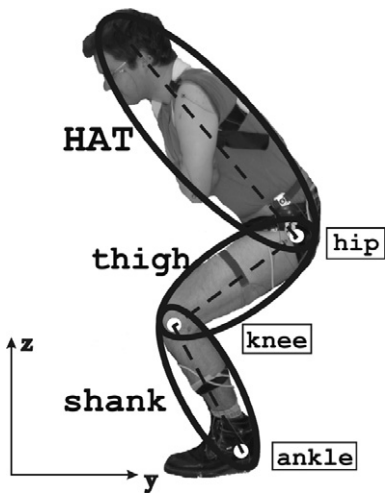

Fig. 1. Standing up motion and three segment human body model.

sumed to be ideal pin joints with no added friction during rotation. The model is in contact with its environment only by the distal end of the shank segment i.e. by subject's feet. The assumption of symmetry of sit-to-stand motion in respect to sagittal plane [14] was adopted in modeling phase. This assumption enables the measurements to be carried out only on one side of the body and results projected on the other side. The symmetry assumption does introduce certain error. The error is sufficiently small in healthy subjects but might have larger values when the method is applied on kinematic data obtained from measurements on impaired subjects.

Mathematical description of three-segment dynamic human body model in sit-to-stand transfer is based on principles of Lagrangian dynamics [19,20]. The Lagrangian method reduces the field of dynamics to a set of simple procedures which are used regardless of the system complexity and relies on a set of *independent generalized coordinates*. The number of independent generalized coordinates must be equal to the number of degrees of freedom of the system. In the developed model the segment orientations (i.e. segment angles) were chosen in respect to horizontal axis (y-axis) as depicted in Fig. 2. The derived model in this configuration demonstrated lower mathematical complexity as compared to models derived using other angle definitions (e.g. angle between two segments).

In the Lagrangian approach the equations of motion for multi-segmental system are derived using

$$\frac{\mathrm{d}}{\mathrm{d}t}\left(\frac{\partial L}{\partial \dot{\Theta}_i}\right) - \frac{\partial L}{\partial \Theta_i} = Q_i, \quad i = 1,2,3 \tag{1}$$

where

L is Lagrangian function ($L = K - V$),
Q_i are generalized forces/moments applied on ith segment defined by $Q_i = \frac{\partial W}{\partial \Theta_i}$ where W is a total work done by applied moments M_1, M_2 and M_3,
K is total kinetic energy of the three-segment system ($K = K_1 + K_2 + K_3$),
V is total potential energy of the three-segment system ($V = V_1 + V_2 + V_3$),
Θ_i is the segment angle defined as the angle between the ith segment and y-axis of the reference coordinate frame (i.e. horizontal).

Using Lagrangian dynamics and model notation from Fig. 2 the equations of motion of the proposed model are derived (see Appendix A). The equations form a non-linear, highly coupled system of differential equations which fully describe three-segment human body model kinematics in standing-up motion. Outputs from the model are angles, angular velocities and angular accelerations from which linear accelerations can be calculated. Model inputs are joint moments M_1, M_2 and M_3 at ankle, knee and hip joint, respectively. These moments are calculated using Newton–Euler inverse dynamic approach [12,20] based on obtained kinematic data and force plate measurements. In the proposed method Newton–Euler inverse dynamic algorithm is positioned inside the EKF iterative loop, but is not part of the EKF algorithm.

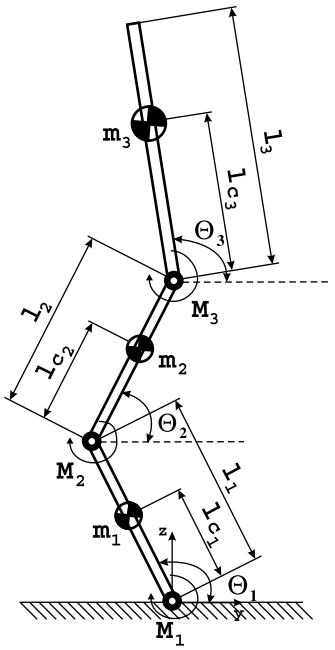

Fig. 2. Notation of three segment human body model parameters.

3. Extended Kalman filter design

In the proposed method Kalman filtering is aimed for fusion of the data acquired through measurements with data obtained from developed dynamic human body model. Kalman filtering is a common approach in multisignal integration tasks [8,12,18,21] whose fundamental drawback is its limitation to linear systems (both stationary and non-stationary). This drawback can be avoided by implementation of Extended Kalman filter (EKF) which adjusts linear approximation of the system state in every iteration. In the EKF, the model is represented by non-linear state space description incorporating state and measurement equations

$$\mathbf{x}_{k+1} = f(\mathbf{x}_k, \mathbf{u}_k, \mathbf{w}_k) \tag{2}$$

$$\mathbf{z}_k = h(\mathbf{x}_k, \mathbf{v}_k) \tag{3}$$

In (2) non-linear function **f** relates the state vector **x** and the input **u** at time step k to the state vector at time step $k + 1$. In (3) measurement vector **h** relates the state vector to the measurement vector $\mathbf{z}_k$. Vectors $\mathbf{w}_k$ and $\mathbf{v}_k$ represent white process and measurement noise, respectively. It is assumed that these noises are Gaussian distributed, have zero mean and that they are uncorrelated.

Before the EKF design process, decomposition of accelerometer signal has been performed in order to differentiate gravitational and dynamic component of accelerometer measurements. These components can easily be distinguished during slower movements when the amplitude of gravity vector is significantly larger than the amplitude of true acceleration vector. During the faster movements, when the motion of the segment to which the accelerometer is attached is not aligned with sensor sensitive axis, gravitational and dynamic component of acceleration can not be distinguished. The sum of the two components represents accelerometer output signal for its sensitive axis. The decomposition of accelerometer output in direction of the z-axis of sensor coordinate frame is presented in Fig. 3.

The sensor angle, which needs to be known for differentiation of two acceleration components, is defined as the angle between sensor z-axis and y-axis of the reference/world coordinate frame. This angle definition was chosen because of sensor placement on body segments and angle definition in dynamic human body model. Also, because of the inertial nature of measurements, the dynamic accelerometer output is opposite to the true direction of segment motion. The decomposition of accelerometer output for z component depicted in Fig. 3 is defined as

$$a_{z_{\mathrm{SENSOR}}} = -(a_{z_{\mathrm{REF}}} \sin\Theta + g \sin\Theta) \tag{4}$$

$$a_{y_{\mathrm{SENSOR}}} = -a_{y_{\mathrm{REF}}} \sin\Theta + g \cos\Theta \tag{5}$$

During the EKF design process several filter architectures were tested keeping in mind computational efficiency and accuracy of the estimates. The chosen filter structure incorporates the state and measurement vectors defined as

$$\mathbf{x}_k = \begin{bmatrix} \Theta_1 \\ \dot{\Theta}_1 \\ \ddot{\Theta}_1 \\ \Theta_2 \\ \dot{\Theta}_2 \\ \ddot{\Theta}_2 \\ \Theta_3 \\ \dot{\Theta}_3 \\ \ddot{\Theta}_3 \end{bmatrix}, \qquad \mathbf{z}_k = \begin{bmatrix} \dot{\Theta}_1 \\ \dot{\Theta}_2 \\ \dot{\Theta}_3 \\ a_{y1} \\ a_{z1} \\ a_{y2} \\ a_{z2} \\ a_{y3} \\ a_{z3} \\ M_1 \\ M_2 \\ M_3 \end{bmatrix}$$

where

Θ_1, Θ_2, Θ_3 – shank, thigh and HAT angles in respect to y-axis,
$\dot{\Theta}_1, \dot{\Theta}_2, \dot{\Theta}_3$ – shank, thigh and HAT angular rates of change i.e. angular velocities,
$\ddot{\Theta}_1, \ddot{\Theta}_2, \ddot{\Theta}_3$ – shank, thigh and HAT angular accelerations,
M_1, M_2, M_3 – ankle, knee and hip joint moments,
a_{yi} – linear acceleration of the ith segment in direction of y-axis of reference coordinate frame,
a_{zi} – linear acceleration of the ith segment in direction of z-axis of reference coordinate frame.

Variables in state and measurement vectors are selected so that they can be measured indirectly or directly by inertial sensors. Directly measured variables are angular velocities and linear accelerations (for every segment), while moments

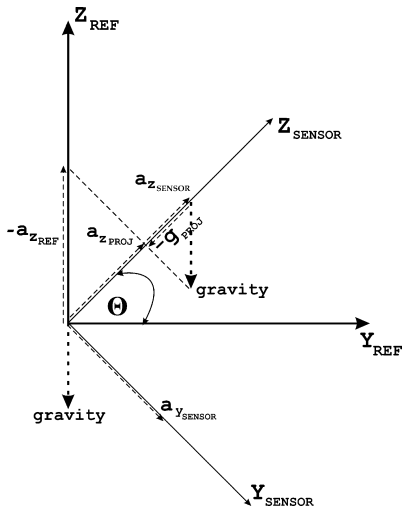

Fig. 3. Accelerometer signal decomposition in direction of *z*-axis.

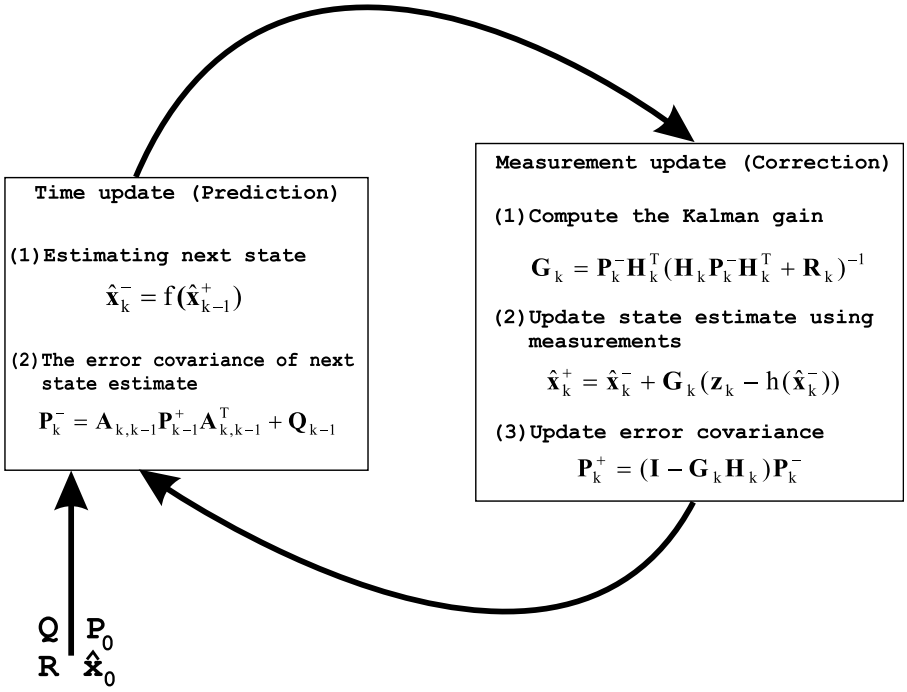

Fig. 4. Extended Kalman filter algorithm.

M_1, M_2 and M_3 are measured indirectly via inverse dynamic calculation using estimated kinematic parameters and measurements from force plate placed under the subject's foot.

The proposed EKF design (see Appendix A) has the advantage that the state equation is linear, while the measurement equation is still highly non-linear. The EKF algorithm is implemented in iterative manner according to [12] as shown in Fig. 4.

The filter is initialized with a state estimate $\hat{\mathbf{x}}_0$ corresponding to system state vector in the initial phase of standing-up.

4. Results

4.1. Results for simulated data

In order to validate the developed dynamic human body model and EKF design, they were implemented in a Matlab–Simulink environment and evaluated by simulated data.

The model (based on (6)–(8) from Appendix A) was constructed in Simulink generating data for description of true model dynamics. The white noise with zero mean was added to data, simulating noisy sensor readings. In the simulation run the joint moments M_1, M_2 and M_3 were *a priori* known, thus Newton–Euler inverse dynamic approach for joint moments calculation was not used. Constructed Simulink model was used in pendulum configuration where the model motion was the result of applied joint moments M_1, M_2 and M_3 and the gravity. The inputs into EKF were simulated sensor readings, while the data about true model dynamics was used for comparison. The sampling frequency in simulation runs was set to 50 Hz in order to match the sampling frequency of the real measurements. The results of simulated three segment model motion in pendulum configuration and corresponding estimated joint angles are presented in Fig. 5.

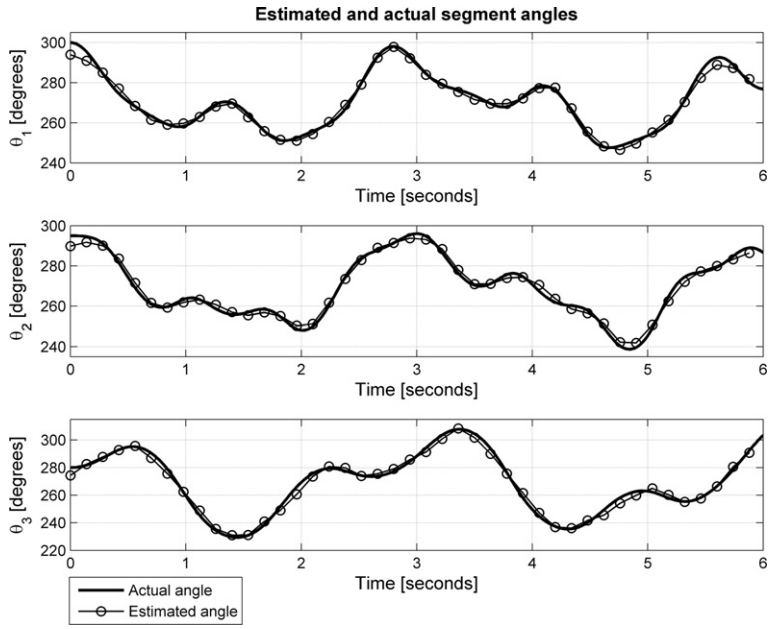

Fig. 5. Comparison of estimated and actual segment angles for simulated data.

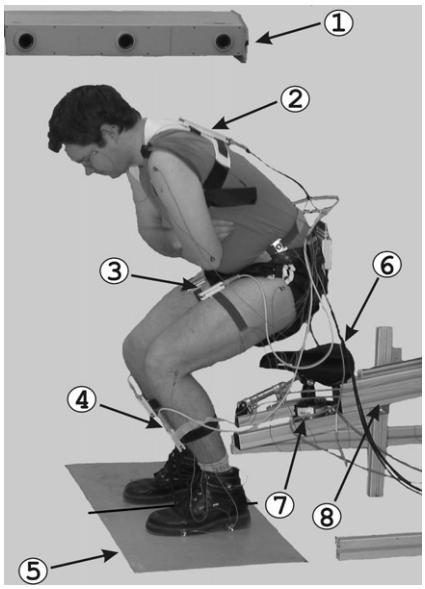

Fig. 6a. Measurement setup: (1) linear infrared cameras, (2) HAT inertial sensing unit, (3) thigh inertial sensing unit, (4) shank inertial sensing unit, (5) AMTI OR6-6-1 force plate, (6) seat, (7) JR3 40E15 force sensor, (8) standing-up robot assistive device.

From presented results it can be seen that constructed three-segment dynamic human body model incorporated in the EKF performed well on simulated data. Root mean square estimation errors for the shank, thigh and HAT segment orientations are 1.75°, 1.68° and 2.47°, respectively. It is interesting to note that all estimation errors have mean values close to zero: −0.41° for the shank, 0.03° for the thigh and −0.35° for the HAT segment. During the simulation trials it was noticed that EKF performance degraded when pendulum oscillated around its equilibrium point. This was attributed to high non-linearities present in segment orientation signals at this time instant.

4.2. Results for measurement data

After validation by simulation, the proposed method was applied on real data. The kinematic parameters in standing-up were measured with the Optotrak 3010 optical motion capture system (Northern Digital Inc., Waterloo, Canada), to which

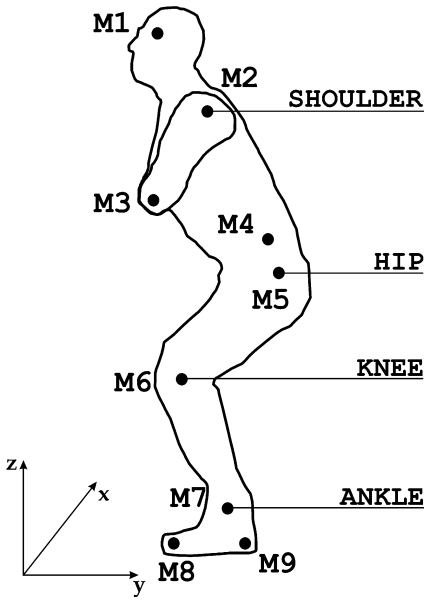

Fig. 6b. Position of Optotrak infrared markers (markers used for calculation of kinematical parameters are additionally marked by the name of body landmark to which they are attached to).

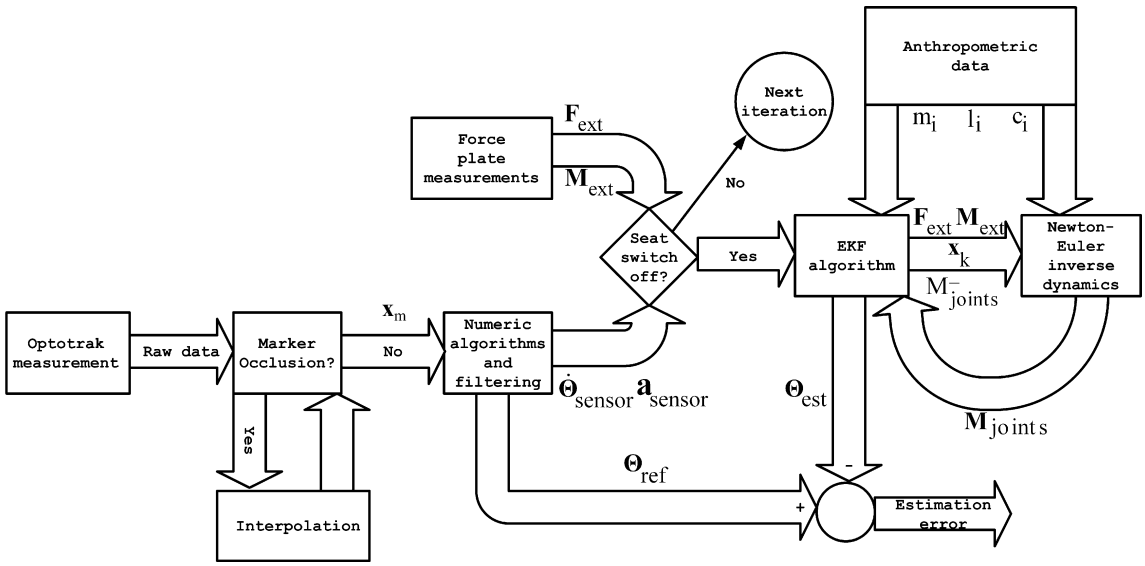

Fig. 7. Conceptual scheme of measurement data processing.

sensor specific noise (e.g. gravitational component of acceleration) was added. Measurements were performed for two different standing up speeds (normal/self-selected and fast/dynamic) with 50 Hz sampling frequency. The sampling frequency selection was determined by performance limitations of the hardware used during the measurements. Measurement setup can be seen in Fig. 6a.

Moreover, in Fig. 6b the placement of Optotrak infrared markers is presented. Positional data measured with Optotrak optical motion analysis system was single and double differentiated to obtain liner velocities and accelerations, respectively [13,15]. This procedure introduced additional numerical error to the signals. During the measurements subject wore inertial sensors for 3D kinematic measurements. Sensors were constructed at the Faculty of Electrical Engineering, University of Ljubljana [11] and were used for verification of sensor specific noises. The AMTI OR6-5-1 force plate (AMTI Inc., Watertown, USA) was placed beneath subject's left foot and was used for the measurements of ground reaction forces and moments acting on the foot during standing-up. The information about external forces and moments is crucial for calculation of joint

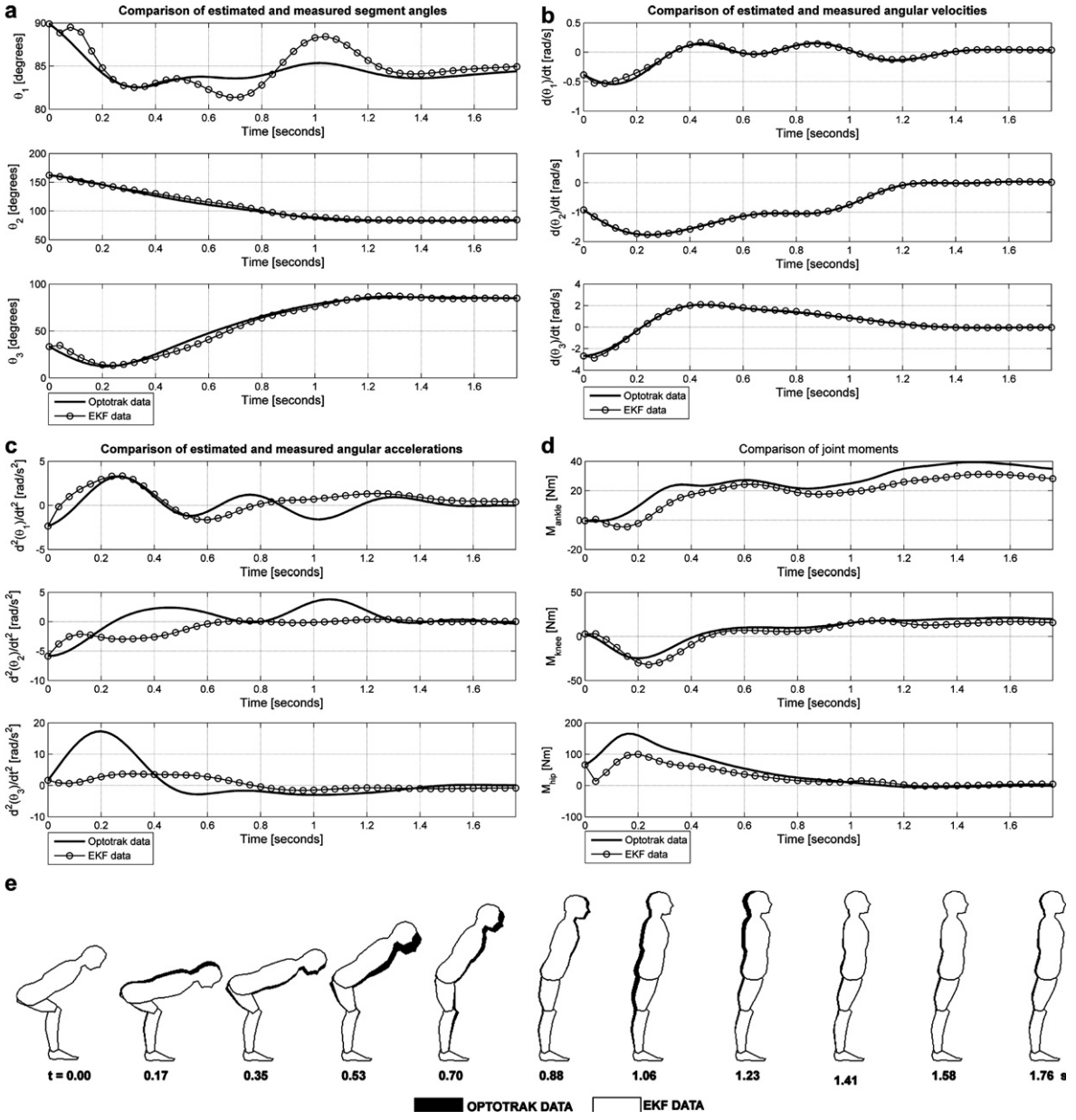

Fig. 8. Comparison of estimated and measured kinematic variables: (a) segment angles, (b) segment angular velocities, (c) segment angular accelerations, (d) joint moments, (e) body motion kinematics presented by black (Optotrak data) and white (EKF data) human body model figures (foot segment has been added for visualization purposes).

Table 1
RMSE of estimated segment orientation angle for complete data set

	Shank RMSE (°)	Thigh RMSE (°)	HAT RMSE (°)
Normal/self-selected standing-up speed			
Measurement 01	6.1	4.1	3.8
Measurement 02	2.1	7.8	6.8
Measurement 03	2.4	5.2	6.8
Measurement 04	3.7	3.5	5.9
Average 1	3.6	5.2	5.8
Fast/dynamic standing-up			
Measurement 05	1.4	2.5	3.2
Measurement 06	4.8	2.6	4.7
Measurement 07	4.9	2.4	5
Measurement 08	3.9	2.1	5
Average 2	3.8	2.4	4.5

moments. Moments in ankle, knee and hip joint (M_1, M_2 and M_3) are not known *a priori*, as in the case of simulated data. They are calculated using Newton–Euler inverse dynamic algorithm which was incorporated in the EKF iterative loop, but was not part of the EKF structure itself. Force sensor 40E15 from JR3 Inc., Woodland, USA was mounted beneath the seat and was used for detection of subject-seat separation. The knowledge of the exact seat-off moment is important because the proposed method is valid only when there is no subject-seat interaction due to model limitations introduced in the modeling phase. The robot assistive device, to which the seat/force sensor system was attached, was used in passive mode for adjustment of seat height and did not provide any assistive force during standing-up.

The subject was in a seated position when measurement recording was started. After two seconds a short beeping sound signaled the test subject to commence with standing-up. The recording was stopped when the subject was in standing position for about two seconds. In total eight measurements were accomplished: four measurements with normal/self-selected speed and four measurements for dynamic standing-up (in which the test subject was instructed to accomplish the sit-to-stand maneuver as fast as possible). The complete calculation procedure for the measurement data is presented in Fig. 7. The acquired raw positional data of infrared markers ($\mathbf{x}_{\mathrm{m}}$) was examined for possible marker occlusions and interpolated in MATLAB environment. From the acquired and interpolated data the kinematic parameters of shank, thigh and HAT were calculated and low pass filtered with fourth order Butterworth filter with 5 Hz cut-off frequency in order to reduce the noise component. In this way, the reference segment angles (Θ_{ref}) were obtained as well as reference segment angular velocities and segment center of mass linear accelerations. To the segmental reference angular velocities signals the simulated gyroscope specific noise was added as drift in time ($\dot{\Theta}_{\mathrm{sensor}}$), and to the reference accelerations signals of segmental centers of masses the simulated accelerometer specific noise was added as gravitational component ($\mathbf{a}_{\mathrm{sensor}}$). The obtained signals were used in the EKF for calculation of estimated segment angles (Θ_{est}) at those times when there was no subject seat interaction (i.e. the seat switch was off). Estimated kinematic parameters ($\mathbf{x}_k$), force plate measurements ($\mathbf{F}_{\mathrm{ext}}$, $\mathbf{M}_{\mathrm{ext}}$) and estimated joint moments from the last iteration ($\mathbf{M}^{-}_{\mathrm{joints}}$) were used as input to the Newton–Euler inverse dynamic algorithm.

As an example, comparison of estimation results with real data for one measurement trial with normal/self-selected standing up speed are presented in Fig. 8, while the averaged results for segment orientation estimation expressed by root mean square errors (RMSE) are presented in Table 1.

5. Discussion

In both the dynamic standing-up and standing-up with normal/self-selected speed, good matching of the actual and estimated segment orientations is observed with the average RMSE values of 3.7° for shank, 3.8° for thigh and 5.2° for HAT segment. Smaller oscillations in orientation estimation can be observed for the shank segment. These oscillations have small amplitudes (less than 5°) and are attributed to the selection of covariance matrices **R** and **Q**, as well as the structure of the EKF. Higher estimation error for segment orientation of thigh and HAT in comparison to shank segment is in our opinion due to higher complexity of dynamic equations that describe the motion of these segments. It should be noted that EKF parameters were defined at the beginning of the trial experiment and were kept constant for all measurement runs with the same speed. On this basis, we conclude that the performance of the EKF estimation is influenced by standing-up speed. Estimation results might be improved if EKF parameters would be automatically adjusted for each particular case. It should be pointed out that perfect matching can not be expected in the accomplished experiment. This is due to the fact that reference Optotrak measurements were presented to the EKF as noisy measurements (matrix **R**).

Estimated angular velocities show good matching with actual values in all instances, while estimated angular accelerations show higher estimation errors compared to other kinematic parameters. We assume that higher angular acceleration estimation error does not cause system fault due to the fact that segment orientation estimation is not affected and thus better angular acceleration estimation can be obtained by numerical derivation. Higher angular acceleration estimation error was attributed to the EKF design, more specifically to the update equation. Better performance of the proposed method in

terms of angular acceleration estimation might be achieved with selection of different EKF parameters. However changing parameters deteriorates the orientation estimation which is the main focus of the proposed model and the method.

If estimated joint moments are compared to the reference values obtained based on Optotrak data, good matching for all joints can be observed. In general, the error in joint moment estimation is largest in the case of knee and hip joints and occurs at the beginning of the estimation. Higher error values are attributed to the fact that at that time higher joint moments are generated by the subject performing sit-to-stand movement. It should be noted that joint moments calculated using an inverse dynamics approach are sensitive to errors in anthropometric data [6,16,17] and even more to errors in the calculation of application point of externally applied forces (i.e. ground reaction forces) [17]. In order to minimize the error due to anthropometric parameters it is suggested that multiple regression body segment parameters of Zatsiorsky and Seluyanov [22] should be used to assess joint kinetics [16]. In our work anthropometric parameters were based on the work of de Leva [5], who adjusted Zatsiorsky–Seluyanov's parameters, thus reducing the influence of the error in anthropometric data on calculated joint moments.

6. Conclusions

The procedure for reconstruction of motion trajectories of shank, thigh and HAT segments in sagittal plane during sit-to-stand maneuvers using three-segment dynamic human body model and Extended Kalman filter is presented. The method is validated on both simulated and measured data. The work is a first step towards the development of a kinematic measurement system based on miniature inertial sensors with application to standing-up re-learning by means of a robot assistive device. For this purpose the dynamic human body model, consisting of three segments (shank, thigh and HAT) connected by joints in the ankle, knee and hip, was constructed using principles of Lagrangian dynamics. Model complexity was reduced by introduction of several assumptions during modeling phase. The EKF data fusion algorithm was used to obtain an estimate of kinematic variables of standing-up motion. Segment orientations, angular velocities and angular accelerations were selected as the EKF system states while the measurement vector consisted of inertial sensor type data and joint moments obtained via Newton–Euler inverse dynamic approach.

The proposed model and the method were first validated by simulations. The Matlab–Simulink model was constructed based on obtained model equations and tested in pendulum configuration. Variables representing inertial sensor readings were extracted from the model and noise added in order to simulate actual sensor measurements. Noisy data represented the input to the EKF algorithm. Obtained results demonstrated good tracking for all segment angles with RMSE of 1.75° for shank, 1.68° for thigh and 2.47° for HAT segment. It is worth nothing that estimation error oscillates around zero i.e. the error mean value is close to zero.

The tracking performance on the measurement data is encouraging, however less accurate than in the case of simulated data with average RMSE of 3.7° for shank, 3.8° for thigh and 5.2° for HAT segments. The reasons for these errors are attributed to: (a) numerical error during Optotrak signal processing, (b) model simplifications, (c) errors in indirectly measured joint moments and (d) not ideal measurement setup (e.g. movement is not restricted to sagittal plane). Method performance in terms of angular velocity estimation is good, but is less accurate in case of angular acceleration which is largely attributed to the proposed EKF structure. The performance of the EKF was dependent on standing-up speed, thus its parameters had to be adjusted accordingly. The EKF parameters were manually adjusted what proved to be time consuming and without guarantee for optimal parameter setting. This emphasized the need for introduction of algorithms for automatic adjustments of EKF parameters [1].

The presented results show that Model Based Inertial Sensing (MoBIS) in robot assisted standing-up is a reliable alternative to optical measurements systems for motion kinematics assessment. To improve method performance in terms of accuracy and reliability, further development (e.g. extensive testing on a group of healthy and impaired subjects, usage of actual inertial sensor measurement signals) is suggested.

Acknowledgements

The authors would like to thank Croatian Ministry of Science, Education and Sports and Slovenian Ministry of Higher Education, Science and Technology for their financial support.

Appendix A

The appendix contains equations of motion of the body segments (Eqs. (6)–(8)) derived from Eq. (1) and model notation from Fig. 2. It also contains the state and measurement equation (Eqs. (9) and (10), respectively) of the EKF which are based on Eqs. (2) and (3).

The equations of motion for the shank, thigh and HAT segments are:

$$\begin{aligned}&\ddot{\Theta}_1(m_1l_{C1}^2+m_2l_1^2+m_3l_1^2+I_{x1})+\ddot{\Theta}_2(m_2l_1l_{C2}+m_3l_1l_2)c(\Theta_1-\Theta_2)+\ddot{\Theta}_3m_3l_1l_{C3}c(\Theta_1-\Theta_3)\\&\quad+\dot{\Theta}_2^2(m_2l_1l_{C2}+m_3l_1l_2)s(\Theta_1-\Theta_2)+\dot{\Theta}_3^2m_3l_1l_{C3}s(\Theta_1-\Theta_3)++g(m_1l_{C1}+m_2l_1+m_3l_1)c\Theta_1=M_1-M_2\end{aligned}\tag{6}$$

for the shank,

$$\ddot{\Theta}_2(m_2l_{C2}^2+m_3l_2^2+I_{x2})+\ddot{\Theta}_1(m_2l_1l_{C2}+m_3l_1l_2)c(\Theta_1-\Theta_2)+\ddot{\Theta}_3m_3l_2l_{C3}c(\Theta_2-\Theta_3)-\dot{\Theta}_1^2(m_2l_1l_{C2}+m_3l_1l_2)s(\Theta_1-\Theta_2)+\dot{\Theta}_3^2m_3l_2l_{C3}s(\Theta_2-\Theta_3)++g(m_2l_{C2}+m_3l_2)c\Theta_2=M_2-M_3 \tag{7}$$

for the thigh and

$$\ddot{\Theta}_3(m_3l_{C3}^2+I_{x3})+\ddot{\Theta}_1m_3l_1l_{C3}c(\Theta_1-\Theta_3)+\ddot{\Theta}_2m_3l_2l_{C3}c(\Theta_2-\Theta_3)-\dot{\Theta}_1^2m_3l_1l_{C3}s(\Theta_1-\Theta_3)-\dot{\Theta}_2^2m_3l_2l_{C3}s(\Theta_2-\Theta_3)+gm_3l_{C3}c\Theta_3=M_3 \tag{8}$$

for the HAT, where

$s \equiv \sin$,
$c \equiv \cos$,
l_i – segment length,
l_{Ci} – position of segment CoM in respect to distal joint,
I_{xi} – segment moment of inertia,
m_i – segment mass.

The state equation of the proposed EKF design is as follows

$$\begin{bmatrix}\dot{\Theta}_1\\ \ddot{\Theta}_1\\ \Theta_1\\ \dot{\Theta}_2\\ \ddot{\Theta}_2\\ \Theta_2\\ \dot{\Theta}_3\\ \ddot{\Theta}_3\\ \Theta_3\end{bmatrix}=\begin{bmatrix}0&1&0&0&0&0&0&0&0\\0&0&1&0&0&0&0&0&0\\0&0&0&0&0&0&0&0&0\\0&0&0&0&1&0&0&0&0\\0&0&0&0&0&1&0&0&0\\0&0&0&0&0&0&0&0&0\\0&0&0&0&0&0&0&1&0\\0&0&0&0&0&0&0&0&1\\0&0&0&0&0&0&0&0&0\end{bmatrix}\cdot\begin{bmatrix}\Theta_1\\ \dot{\Theta}_1\\ \ddot{\Theta}_1\\ \Theta_2\\ \dot{\Theta}_2\\ \ddot{\Theta}_2\\ \Theta_3\\ \dot{\Theta}_3\\ \ddot{\Theta}_3\end{bmatrix} \tag{9}$$

while measurement equations is defined as

$$\begin{bmatrix}h_1\\h_2\\h_3\\h_4\\h_5\\h_6\\h_7\\h_8\\h_9\\h_{10}\\h_{11}\\h_{12}\end{bmatrix}=\begin{bmatrix}\dot{\Theta}_1\\ \dot{\Theta}_2\\ \dot{\Theta}_3\\ (c_1\ddot{\Theta}_1s\Theta_1c_1\dot{\Theta}_1^2c\Theta_1)s\Theta_1+gc\Theta_1\\ -(c_1\ddot{\Theta}_1c\Theta_1-c_1\dot{\Theta}_1^2s\Theta_1)s\Theta_1-gs\Theta_1\\ (l_1\ddot{\Theta}_1s\Theta_1+l_1\dot{\Theta}_1^2c\Theta_1+c_2\ddot{\Theta}_2s\Theta_2+c_2\dot{\Theta}_2^2c\Theta_2)s\Theta_2+gc\Theta_2\\ -(l_1\ddot{\Theta}_1c\Theta_1-l_1\dot{\Theta}_1^2s\Theta_1+c_2\ddot{\Theta}_2c\Theta_2-c_2\dot{\Theta}_2^2s\Theta_2)s\Theta_2-gs\Theta_2\\ (l_1\ddot{\Theta}_1s\Theta_1+l_1\dot{\Theta}_1^2c\Theta_1+l_2\ddot{\Theta}_2s\Theta_2+l_2\dot{\Theta}_2^2c\Theta_2+c_3\ddot{\Theta}_3s\Theta_3+c_3\dot{\Theta}_3^2c\Theta_3)s\Theta_3+gc\Theta_3\\ -(l_1\ddot{\Theta}_1c\Theta_1-l_1\dot{\Theta}_1^2s\Theta_1+l_2\ddot{\Theta}_2c\Theta_2-l_2\dot{\Theta}_2^2s\Theta_2+c_3\ddot{\Theta}_3c\Theta_3-c_3\dot{\Theta}_3^2s\Theta_3)s\Theta_1-gs\Theta_1\\ M_2+K_{11}\ddot{\Theta}_1+K_{12}\ddot{\Theta}_2c(\Theta_1-\Theta_2)+K_{13}\ddot{\Theta}_3c(\Theta_1-\Theta_3)+K_{14}\dot{\Theta}_2^2s(\Theta_1-\Theta_2)+K_{15}\dot{\Theta}_3^2s(\Theta_1-\Theta_3)+K_{16}c\Theta_1\\ M_3+K_{22}\ddot{\Theta}_2+K_{21}\ddot{\Theta}_1c(\Theta_1-\Theta_2)+K_{23}\ddot{\Theta}_3c(\Theta_2-\Theta_3)-K_{24}\dot{\Theta}_1^2s(\Theta_1-\Theta_2)+K_{25}\dot{\Theta}_3^2s(\Theta_2-\Theta_3)+K_{26}c\Theta_2\\ K_{33}\ddot{\Theta}_3+K_{31}\ddot{\Theta}_1c(\Theta_1-\Theta_3)+K_{32}\ddot{\Theta}_2c(\Theta_2-\Theta_3)-K_{34}\dot{\Theta}_1^2s(\Theta_1-\Theta_3)-K_{35}\dot{\Theta}_2^2s(\Theta_2-\Theta_3)+K_{36}c\Theta_3\end{bmatrix} \tag{10}$$

In (10) meaning of the parameters is as follows

$s \equiv \sin$
$c \equiv \cos$
$K_{11}=m_1l_{C1}^2+m_2l_1^2+m_3l_1^2+I_{x1}$
$K_{12}=K_{14}=K_{21}=K_{24}=m_2l_1l_{C2}+m_3l_1l_2$
$K_{13}=K_{15}=m_3l_1l_{C3}$
$K_{16}=g(m_1l_{C1}+m_2l_1+m_3l_1)$
$K_{22}=m_2l_{C2}^2+m_3l_2^2+I_{x2}$
$K_{23}=K_{25}=K_{32}=K_{35}=m_3l_2l_{C3}$
$K_{26}=g(m_2l_{C2}+m_3l_2)$
$K_{31}=K_{34}=m_3l_1l_{C3}$
$K_{33}=m_3l_{C3}^2+I_{x3}$
$K_{36}=m_3gl_{C3}$

References

[1] P. Abbel, A. Coates, M. Montemerlo, A. Ng, S. Thun, Discriminative training of Kalman filters, in: Proceedings of Robotics: Science and Systems I, Cambridge, USA, 2005, pp. 289–296.
[2] E. Bachmann, X. Yun, C. Peterson, An investigation of the effects of magnetic variations on inertial/magnetic orientations, in: Proceedings of 2004 IEEE International Conference on Robotics and Automation (ICRA'04), Barcelona, Spain, 2004, pp. 1115–1122.
[3] M. Boonstra, M. van der Slikke, N. Keijsers, R. van Lummel, M. de Waal Malefijt, N. Verdonschot, The accuracy of measuring the kinematics of rising from chair with accelerometers and gyroscopes, Journal of Biomechanics 39 (2) (2006) 354–356.
[4] S.S. Coghlin, B.J. McFadyen, Transfer strategies used for rise from a chair in normal and low back pain subjects, Clinical Biomechanics 9 (2) (1994) 85–92.
[5] P. de Leva, Adjustment to Zatsiorsky–Seluyanov's segment inertia parameters, Journal of Biomechanics 29 (9) (1996) 1223–1230.
[6] K.J. Ganley, C.M. Powers, Determination of lower extremity anthropometric parameters using dual energy X-ray absorptiometry: the influence of net joint moments during gait, Clinical Biomechanics 19 (1) (2004) 50–56.
[7] D. Giansanti, G. Maccioni, V. Macellari, The development and test of a device for the reconstruction of 3-D position and orientation by means of kinematic sensor assembly with rate gyroscope and accelerometers, IEEE Transactions on Biomedical Engineering 52 (7) (2005) 1271–1277.
[8] M. Haid, J. Breitenbach, Low cost inertial orientation tracking with Kalman filter, Applied Mathematics and Computation 153 (2) (2004) 567–575.
[9] H. Hemami, V.C. Jaswa, On a three-link model of the dynamics of standing up and sitting down, IEEE Transactions on System, Man and Cybernetics 8 (1978) 115–120.
[10] D. Jurman, M. Jankovec, R. Kamnik, M. Topič, Calibration and data fusion solution for the miniature attitude and heading reference system, Sensors and Actuators A 138 (2007) 411–420.
[11] R. Kamnik, J. Musić, H. Burger, M. Munih, T. Bajd, Design of inertial motion sensor and its usage in biomechanical analysis, in: Proceedings of 4th International Conference on Electrical and Power Engineering, Isai, Romania, 2006, pp. 511–516.
[12] R. Kamnik, T. Bajd, Human voluntary activity integration in the control of a standing-up rehabilitation robot: a simulation study, Medical Engineering and Physics 29 (9) (2007) 1019–1029.
[13] A. Kralj, J. Jaeger, M. Munih, Analysis of standing up and sitting down in humans: definitions and normative data presentation, Journal of Biomechanics 23 (11) (1990) 1123–1138.
[14] T. Lundin, M. Grabiner, D. Jahnigen, On the assumption of bilateral lower extremity joint moment symmetry during the sit-to-stand tasks, Journal of Biomechanics 28 (1) (1995) 109–112.
[15] R.E. Mayagoitia, A.V. Nene, P. Veltink, Accelerometer and rate gyroscope measurement of kinematics: an inexpensive alternative to optical motion analysis system, Journal of Biomechanics 35 (4) (2002) 537–542.
[16] G. Rao, D. Amarantini, E. Berton, D. Favier, Influence of body segments' parameters estimation models on inverse dynamics solutions during gait, Journal of Biomechanics 39 (8) (2006) 1531–1536.
[17] M.P.T. Silva, J.A.C. Ambrósio, Sensitivity of the results produced by the inverse dynamic analysis of a human stride to perturbed input data, Gait and Posture 19 (1) (2004) 35–49.
[18] D. Roetenberg, H. Luinge, C. Baten, P. Veltink, Compensation of magnetic disturbances improves inertial and magnetic sensing of human body segment orientation, IEEE Transactions on Neural System and Rehabilitation Engineering 13 (3) (2005) 395–405.
[19] D.A. Wells, Lagrangian dynamics, McGraw-Hill Book Company., New-York, USA, 1967.
[20] D.A. Winter, Biomechanics and motor control of human movement, 2nd ed., Wiley Interscience, New York, USA, 1990.
[21] X. Yun, E. Bachmann, Design, implementation and experimental results of quaternion-based Kalman filter for human body motion tracking, IEEE Transactions on Robotics 22 (6) (2006) 1216–1227.
[22] V. Zatsiorsky, V. Seluyanov, The mass and inertial characteristics of main segments of the human body, in: Biomechanics VIII-B, Human Kinetics, Champaign, USA, 1983, pp. 1152–1159.
[23] R. Zhu, Z. Zhou, A real-time articulated human motion tracking using tri-axis inertial/magnetic sensor package, IEEE Transactions on Neural Systems and Rehabilitation Engineering 12 (2) (2004) 295–302.